DEVELOPMENT OF CATALYSTS FOR BIOMASS TRANSFORMATION

M.Sc. Thesis

By

Narottam Sahu

Supervised by: **Prof. Sanjay K. Singh**



DEPARTMENT OF CHEMISTRY

INDIAN INSTITUTE OF TECHNOLOGY INDORE

May 2026

DEVELOPMENT OF CATALYSTS FOR BIOMASS TRANSFORMATION

A THESIS

Submitted in partial fulfilment of the
requirements for the award of the degree
of
Master of Science

by

Narottam Sahu



DEPARTMENT OF CHEMISTRY
INDIAN INSTITUTE OF TECHNOLOGY INDORE

May 2026

INDIAN INSTITUTE OF TECHNOLOGY INDORE

CANDIDATE'S DECLARATION

I hereby certify that the work which is being presented in the thesis entitled **DEVELOPMENT OF CATALYSTS FOR BIOMASS TRANSFORMATION** in the partial fulfilment of the requirements for the award of the degree of **MASTER OF SCIENCE** and submitted in the **DEPARTMENT OF CHEMISTRY, Indian Institute of Technology Indore**, is an authentic record of my own work carried out during the time period from July 2025 to May 2026 under the supervision of Prof. Sanjay Kumar Singh, Professor, Indian Institute of Technology Indore.

The matter presented in this thesis has not been submitted by me for the award of any other degree of this or any other institute.

14/05/2026

Signature of the student with date

Narottam Sahu

This is to certify that the above statement made by the candidate is correct to the best of my knowledge.

Signature of the Supervisor

Prof. Sanjay Kumar Singh

Narottam Sahu has successfully given his M.Sc. Oral Examination held on **11th May 2026**.

11.05.2026

Signature of Supervisor of M.Sc. thesis

Prof. Sanjay Kumar Singh

ACKNOWLEDGEMENTS

It is with immense pleasure that I convey my heartfelt gratitude to my esteemed supervisor, Prof. Sanjay Kumar Singh. His invaluable guidance and direction have been a constant source of inspiration for me.

I am genuinely thankful to the Department of Chemistry at IIT Indore for affording me the privilege to embark on my M.Sc. Research Project. My appreciation extends to Dr. Umesh A Kshirsagar, the Head of the Department of Chemistry at the Indian Institute of Technology Indore.

I would also like to express my sincere gratitude to the dedicated technical staff at the Sophisticated Instrumentation Centre (SIC) at IIT Indore. Their expertise has been instrumental in the progression of my research.

Furthermore, I extend my profound thanks to all my Lab seniors- Dr. Pooja Prajapati, Tushar A. Kharde, Jayashree Parthiban, Khanindra Kalita, Shivam Mishra, Kanhaiya Singh, Aditi Gautam - It is through their support and guidance that I have been able to navigate my work with confidence and efficiency. At last, I would like to thank my family members and friends- Meet, kartik, Anamika, Divyanshi, Anahita, Chhagan and all my classmates for always supporting me.

NAROTTAM SAHU
M.Sc. (Chemistry)
Roll No: 2403131020

ABSTRACT

Lignin is the most abundant renewable source of aromatic carbon, but it is mostly used as a low-value thermal fuel. Its complex structure, which includes β-O-4, α-O-4, 4-O-5, and different C-C linkages, makes selective depolymerization challenging. However, converting lignin can lead to valuable hydrocarbons, from gasoline to aviation-grade fuels. A successful approach involves breaking ether bonds to produce phenolic intermediates, which can then be turned into fully saturated alkanes through hydrodeoxygenation. In this study, we looked at breaking ether linkages with both noble and non-noble metal catalysts on hierarchical supports like HZ4A zeolite and hierarchical silica. Because native lignin has a complex structure, we used a series of model compounds: 2-Phenoxy-1-phenylethanone and its analogues to represent β-O-4 linkages, benzyl phenyl ether for α-O-4, and diphenyl ether for 4-O-5 linkages. We also included guaiacol and cinnamaldehyde to represent monolignol-type aromatic precursors in this study. Our evaluations of catalytic performance showed patterns in bond-breaking efficiency and product selectivity based on the metal-support combination. This suggests that both acid-metal synergy and pore structure are important for improving the conversion of lignin model compounds.

NOMENCLATURE

°C	Degree Celsius
h	Hour
mL	Millilitre
min	Minutes
mmol	Millimole
mg	Milligram
pH_2	Pressure of H_2 gas
RT	Room Temperature
Ref.	Reference
T	Temperature
t	Time

ACRONYMS

$CDCl_3$	Chloroform-d
Conv.	Conversion
CTAB	Cetyltrimethylammonium bromide
D_2O	Deuterium oxide
FTIR	Fourier transform infrared spectroscopy
GC-MS	Gas chromatography-mass spectrometry
H_2	Hydrogen
HDO	Hydrodeoxygenation
HS	Hierarchical Silica
Ni	Nickel
$Ni(NO_3)_2 \cdot 6H_2O$	Nickel nitrate hexahydrate
NMR	Nuclear magnetic resonance
P-XRD	Powder X-ray diffraction
TEOS	Tetraethyl orthosilicate
TMS	Tetramethyl silane
$NaBH_4$	Sodium Borohydride
amu	Atomic Mass Unit

LIST OF FIGURES

Figure 1 Different sources of lignin

Figure 2 Structural part of lignin polymer

Figure 3 Structure of monolignols: (a) Coumaryl alcohol, (b) Coniferyl alcohol, (c) Sinapyl alcohol

Figure 4 Model compounds used for catalytic studies

Figure 5 Preparation of HZ4A.

Figure 6 Preparation of Ni/HZ4A and Ni/HS

Figure 7 Preparation of Ru/HZ4A.

Figure 8 Flowchart extraction of soda lignin from wheat straw

Figure 9 Catalytic reaction procedure

Figure 10 FTIR of Extracted Lignin

Figure 11 FTIR of (a) HZ4A, (b) Ni/HZ4A, (c) Hierarchical silica, (d) Ru/HZ4A

Figure 12 P-XRD of (a) HZ4A, (b) Reported HZ4A, (c) HS, (d) reported HS

Figure 13 Pore diameter (a,b), and BET data (c,d) of catalysts

Figure 14 GC-MS data of BPE reaction with HZ4A in H_2 in 100 mL reactor

Figure 15 GC-MS data of BPE reaction with HZ4A in H_2

Figure 16 GC-MS data of BPE reaction with HZ4A in N_2

Figure 17 GC-MS data of BPE reaction with Ni/HS in HZ4A

Figure 18 GC-MS data of 2-phenoxy-1-phenylethan-1-one reaction with HZ4A in H_2

Figure 19 GC-MS data of 2-Phenoxy-1-phenylethanone reaction with Ni/HZ4A in H_2

Figure 20 GC-MS data of 2-Phenoxy-1-phenylethanone reaction with Ni/HZ4A in H_2

Figure 21 GC-MS data of reaction cinnamyl alcohol with HZ4A

Figure 22 GC-MS data of 2-methoxycinnamaldehyde reaction with Ni/HZ4A

Figure 23 GC-MS data of 2-methoxycinnemaldehyde reaction with HS

Figure 24 GC-MS data of Lignin with HZ4A catalyst

Figure 25 Graphical idea on Lignin to fuel

LIST OF TABLES

Table 1 Literature reports on biomass transformation with noble metal catalysts

Table 2 Literature reports on the biomass transformation of model lignin with Ni catalysts.

TABLE OF CONTENTS

- Abstract vi
- Nomenclature vii
- Acronyms viii
- List of figures ix
- List of tables xi

Chapter 1: Introduction 1

1.1. General Introduction

1.2. Literature review

1.3. Objective of the project

Chapter 2: Materials and methods 9

2.1. Chemicals

2.2. Preparation of HZ4A

2.3. Preparation of Hierarchical Silica

2.4. Preparation of Ni/Support

2.5. Lignin Extraction

2.6. Synthesis of β-O-4 model compounds

2.7. Catalytic Reaction

Chapter 3: Results and Discussions 15

3.1. Characterizations

3.2. Reaction of Benzyl Phenyl Ether (α-O-4)

3.3. Reaction of Diphenyl Ether (4-O-5)

3.4. Reaction of 2-phenoxy-1-phenylethanone (β-O-4)

3.5. Reaction of monolignols model compounds

3.6. Reaction of Extracted Lignin

Chapter 4: Conclusion and future scope 24

Chapter 5: References 25

CHAPTER 1

INTRODUCTION

1.1. General Introduction

The ever-expanding industry, with an exponential increase in energy consumption over the last century, largely driven by fossil fuels, poses an alarming threat to the environment. Since it is non-renewable and leaves a carbon footprint, sustainable alternative sources are now being researched worldwide. Fuel produced from biomass feedstock has shown promising results in both fulfilling requirements and processing waste.[1,2]

Biomass is organic matter from plants, animals, or microorganisms that can be used as a renewable source of energy or raw material. In plant biomass, Lignocellulose is the structural material, and it is one of the most abundant renewable organic substances produced on Earth.[3]



Figure 1. Different sources of Lignin

A wide range of materials, including agricultural residues such as wheat and rice straw, industrial by-products like sawdust and wood chips, and municipal solid waste, contribute to the global lignocellulose pool (Figure 1).[4] These sources are inexpensive, renewable, and often underutilised, making them attractive for sustainable applications.

Lignocellulose is the major non-food component of biomass, tightly associated within a complex matrix composed of cellulose (40-60%), hemicellulose (10-30%), and lignin (20-35%). Lignin is a complex, irregular polymer built from three aromatic units- coniferyl (G), Sinapyl (S), and Coumaryl (H) alcohols; connected by ether and C-C linkage. In which *β*-O-4 (*β*-aryl ether) bonds, making up about 45-60% of all connections.[5] The *β*-5 (phenyl-coumaran) linkages typically account for 6-12%, while *β*-*β* (Pinoresinol) bonds contribute around 4-8%. More stable linkages, such as 5-5 (biphenyl) and *α*-O-4 (alkyl-aryl ether), each make up roughly 3-9%. These proportions vary with plant type but consistently show *β*-O-4 as the major linkage (Figure 2).[6]

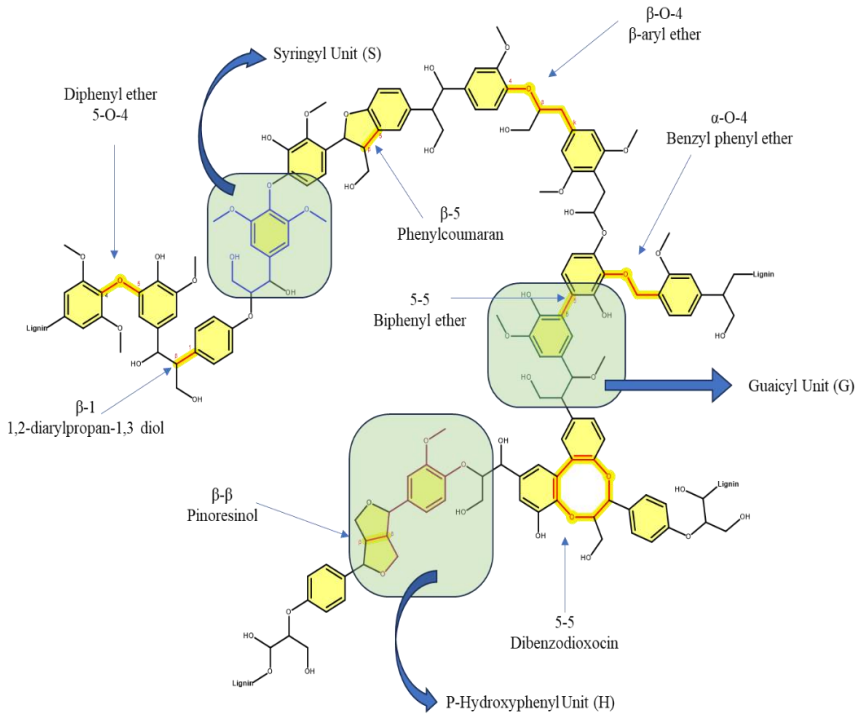


Figure 2. Structural part of lignin polymer

Lignin can be upgraded to hydrocarbons mainly through hydrodeoxygenation (HDO) and hydrogenation. HDO removes oxygen from lignin-derived molecules to form cleaner aromatic or aliphatic hydrocarbons, while hydrogenation focuses on saturating and stabilising lignin fragments.[7] Together, these routes convert complex lignin into fuel-range, energy-rich hydrocarbons. Taking inspiration from this idea, this work focuses on developing a catalyst to convert one of the major biomass wastes, lignin, into fuel.

1.2. Literature Review

The relative abundance of lignin in different units depends on plant species- for example, softwoods typically contain around 90-95% G units and 5-10% H units, and hardwoods have a mixture of approximately. 25-50% G and 50-75% S units, while grasses contain all three in varying proportions.[8]

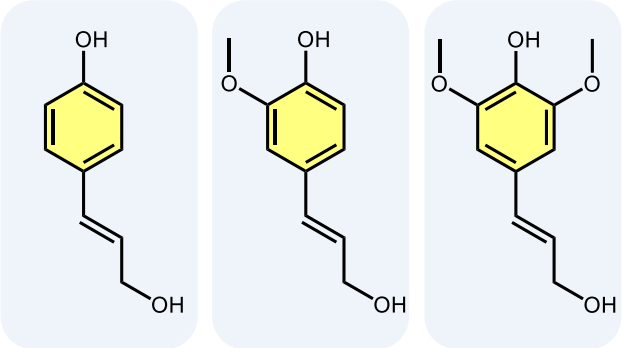


Figure 3 Structure of Monolignols: (a) Coumaryl alcohol, (b) Coniferyl alcohol, (c) Sinapyl alcohol

Lignin has significant mechanical strength and rigidity, making it highly resistant to depolymerisation. Consequently, early research into its use was limited, and many industries considered it waste. Catalytic reactions are often studied using lignin model compounds because real lignin is highly complex, heterogeneous, and difficult to characterise during reactions. Its irregular structure, ether linkages, and variability across biomass sources make it challenging to pinpoint the underlying catalytic mechanism. Model compounds, by contrast, are simple molecules that represent specific linkages or structural motifs found in lignin. This approach helps us understand fundamental reaction pathways, identify active sites, and evaluate catalyst selectivity under controlled conditions. Insights gained from these simplified systems can then be correlated with real lignin, since the same key functional groups and bond types are present.

Simplified β-O-4 analogues, such as phenethyl phenyl ether and 2-phenoxy-1-phenylethanol, retain the essential ether connectivity while reducing structural complexity.[9] For α-O-4 linkages, benzyl phenyl ether and its derivatives serve as practical model compounds, capturing the key α-aryl ether bond in a more minimal molecular framework.[10]

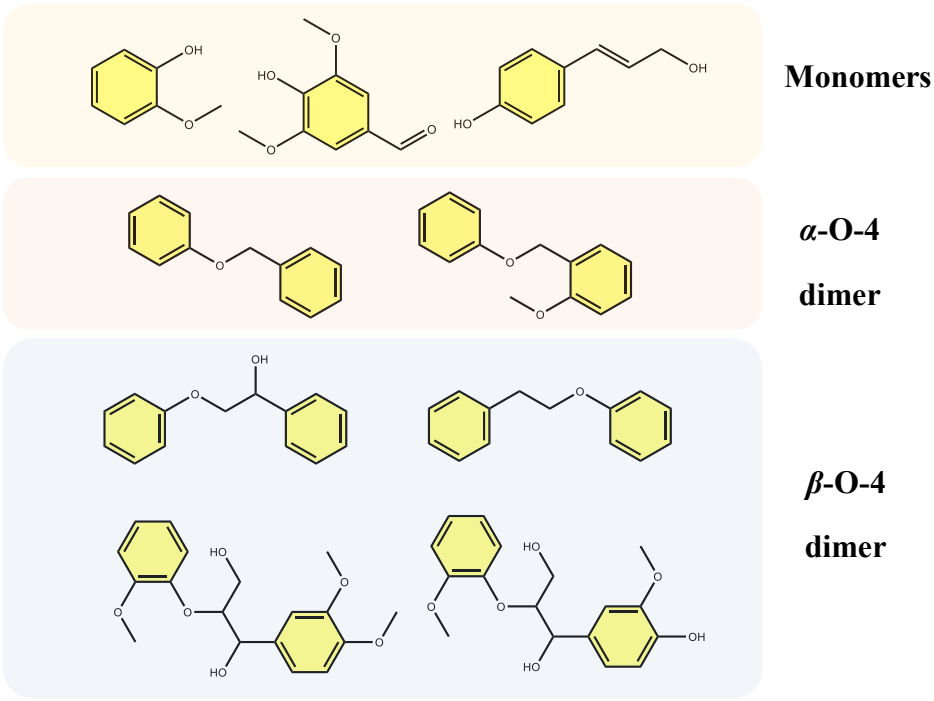


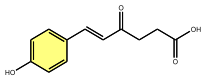
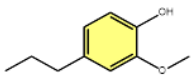
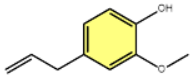
Figure 4 Model compounds used in Catalytic studies

Among the various lignin-degradation methods, acid-base catalysis is one of the most widely studied. Konnerth *et al*. demonstrated that strong bases, such as sodium hydroxide, can effectively cleave C-O bonds in lignin model dimers in water with high selectivity.[11] Bengoechea *et al.* reported that the stable Lewis acidity of alumina supports improves lignin conversion, highlighting that appropriate acidic conditions are essential for efficient lignin depolymerisation.[12]

With the advancement of green chemistry, solid acid-base catalysts have gained significant interest because they are less corrosive and offer high catalytic selectivity, particularly by reducing the formation of tar by-products. Among these, Noble metals and transition metals on various supports are observed as highly effective catalysts for lignin conversion, and several catalysts have been developed that support this research direction.

In 2018, Chen *et al*. developed a Pd/C catalyst that converted (E)-6-(4-hydroxyphenyl)-4-oxohex-5-enoic acid, its 3-methoxy, and 3,5-dimethoxy derivatives into C12 alkanes with maximum conversions of 81%, 87%, and 68%, respectively.[13] Li *et al*. reported that Ru/H-*β* exhibited strong hydrodeoxygenation and hydrogenation due to well-dispersed Ru particles, favourable pore structure, and Bronsted/Lewis

Table 1: Literature reports on biomass transformation with noble metal

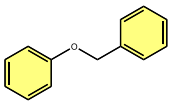
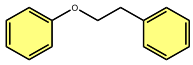
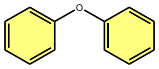
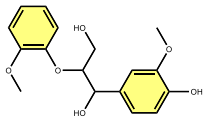
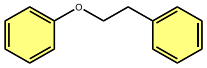
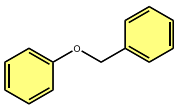
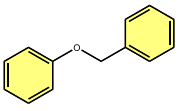
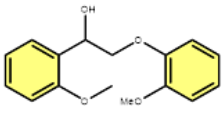
#	Substrate	Catalyst	Solvent	Reaction Conditions	Product (yield%)	Ref.
1		Pd/C	MeOH	RT, 0.1 MPa H_2, 2 h	C12 alkanes (81)	13
2		Ru/H-*β*	H_2O	140 °C, 40 bar H_2, 8 h.	C9 alkanes (95)	14
3		Ru/C and Nb_2O_5	H_2O + MeOH	250 ºC, 6 bar H_2, 12 h.	C9 alkanes (76)	15
4		Ru/CNT	H_2O	270 °C, 40 bar H_2, 1 h	C9 alkanes (29)	16
5		Ru/C Fe_2O_3-600	Hexadecane	275 °C, 50 bar H_2, 2 h	C9 alkanes (80)	17

acid sites, achieving 95% yield of propylcyclohexane from 4-n-propylguaiacol.[14] Li *et al.* showed lignin monomers could be converted to C9 hydrocarbons using Ru/C and Nb_2O_5 at 250 °C in water with methanol, yielding 76% propylcyclohexane via fully deoxygenated products.[15] Ha et al. used Ru/MWCNT in water for hydroconversion of 2-methoxy-4-propylphenol (40 bar H_2, 270 °C, 1 h), producing cycloalkanes suitable for aviation fuel with around 29% yield.[16] Bjelić *et al.* demonstrated Ru/C- Fe_2O_3-600 efficiently converted eugenol in hexadecane (50 bar H_2, 275 °C, 2 h) to n-propylcyclohexane with 80% yield.[17]

Despite their efficiency, noble metals are costly and scarce, so research has shifted toward cheaper, more abundant transition metals that offer more sustainable and scalable catalytic options. In 2020, Phan *et al.* reported that Ni/SiO_2 effectively cleaved benzyl phenyl ether (α-O-4) in water at 120 °C for 2 h, yielding phenol and toluene in 50%.[18] In the same paper, they demonstrated that the same Ni/SiO_2 catalyst could also convert 2-phenethyl phenyl ether (β -O-4) under identical aqueous conditions, affording phenol and ethylbenzene with a 48% yield. Additionally, they showed that diphenyl ether (4-O-5) underwent selective C-O bond cleavage over the same catalyst in water at 120 °C, forming benzene and cyclohexanol with a notably higher 65% yield. Moving to a different support, Song *et al*. established that Ni/CeO_2 operated in water at 180 °C and 20 bar H_2 for 4 h could efficiently convert the β-O-4 dimer into guaiacol and propyl guaiacol with a 70% yield.[19] Furthermore, Zhu *et al*. demonstrated that Ni/C in methanol at 220 °C and 20 bar H_2 selectively produced phenol and ethylbenzene from phenethyl phenyl ether with a 65% yield.[20]

In another contribution, Biswas *et al.* showed that Ni/ZrO_2 used in water at 180 °C and 20 bar H_2 achieved highly efficient cleavage of benzyl phenyl ether, delivering phenol and toluene in 82% yield.[21] Likewise, Zhu *et al*. investigated Ni/HZSM-5 under harsher conditions (250 °C, 40 bar H_2) and observed the conversion of a lignin model mixture into phenol and toluene with a 45.5% yield in 30 min.[22]

Table 2: Literature reports on biomass transformation of model lignin with Ni Catalysts

#	Model Compound	Catalyst	Solvent	Reaction Conditions	Main Products (Yield%)	Ref
1		Ni/SiO_2	H_2O	120 °C, 2 h	Phenol + Toluene (50%)	18
2		Ni/SiO_2	H_2O	120 °C, 2 h	Phenol + Ethyl-benzene (48%)	18
3		Ni/SiO_2	H_2O	120 °C, 2 h	benzene + Cyclo-hexanol (65%)	18
4		Ni/CeO_2	H_2O	180 °C, 20 bar H_2, 4 h	Guaiacol + propyl guaiacol (70%)	19
5		Ni/C	MeOH	220 °C, 20 bar H_2, 6 h	Phenol + Ethyl-benzene (65%)	20
6		Ni/ZrO_2	H_2O	180 °C, 20 bar H_2, 3 h	Phenol + Toluene (82%)	21
7		Ni/ HZSM-5	H_2O	250 °C, 40 bar H_2, 30 min	Phenol + Toluene (45.5%)	22
8		Ni-CeO_2/H-ZSM-5	EtOH	150 °C, 10 bar H_2	Ethyl-benzene (63%)	23

Lin *et al.* demonstrated that the bifunctional Ni-CeO_2/H-ZSM-5 catalyst in ethanol at 150 °C and 10 bar H_2 selectively produced ethylbenzene in 63% yield from phenethyl phenyl ether, emphasizing the diverse and tuneable performance of Ni-based catalysts supported on different materials.[23]

HZ4A (LTA framework) contains moderate Bronsted acid sites. Even if 4 Å pore openings. It can be a good option as a catalyst support because its high aluminium content and resulting abundance of exchangeable sites allow the introduction of Bronsted acidity through proton exchange. Its highly hydrophilic and polar surface provides strong interactions with oxygenated biomass-derived molecules, improving adsorption and activation of polar substrates.[24] Additionally, another material was considered as support, which is Hierarchical silica. Unlike zeolites, it is largely non-Lewis acidic but provides a high surface area and interconnected micro/mesoporous structure that greatly enhances mass transport and promotes uniform metal dispersion for hydrogenolysis and hydrogenation pathways.[25]

1.3. Objective of the project

In this study, Benzyl phenyl ether and phenethyl phenyl ether derivatives were used as lignin model compounds for the α-O-4. HZ4A zeolite was selected with a Si/Al ratio of 60, and incorporated with Ni (10 wt.%) and Ru (5 wt %) by the deposition-precipitation (DP) method to prepare Ni/HZ4A, Ru/HZ4A catalyst. Similarly, Ni (10 wt %) was loaded on hierarchical silica to make Ni/HS catalyst. The efficiency of cleaving the C-O bond in typical lignin model compounds was investigated.

CHAPTER 2

MATERIALS AND METHODS

2.1. Chemicals

All reagents and solvents for the synthesis and analysis were purchased from Sigma Aldrich, and TCI. Used as received without any further purifications. ^{1}H NMR was recorded in deuterated solvent ($CDCl_3$, D_2O) using Bruker Advance 400 and Bruker Ascend 500. IR spectra were recorded on a Bruker IR instrument. Rigaku SmartLab XRD instrument was used for P-XRD analysis. Micromeritics TriStar II Plus for BET analysis. GC-MS was done in a GC-MS QP 2010 Ultra mass spectrometer from Shimadzu.

2.2. Preparation of HZ4A

HZ4A was prepared by following the previously reported method.[24] 1 g of preheated Zeolite 4A in 75 mL of aqueous urea solution (urea: zeolite = 1:3), and stirring the mixture for 20 min at room temperature. The resulting suspension was transferred to a 100 mL Teflon-lined autoclave and subjected to hydrothermal treatment at 220 °C for 12 h. After naturally cooling to room temperature, the solid product was collected by centrifugation the material was calcined in a tubular furnace at 350 °C for 12 h with a heating rate of 5 °C min-1 to obtain HZ4A.

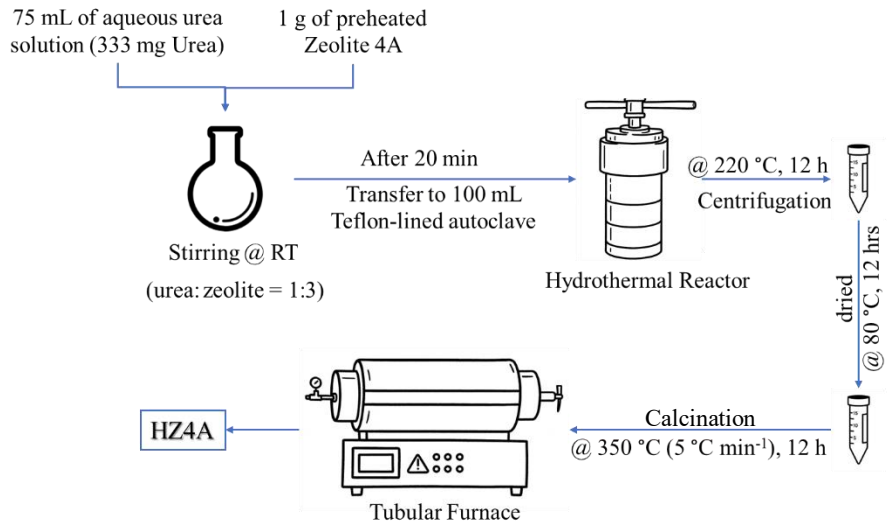


Figure 5. Preparation of the HZ4A

2.3. Preparation of Hierarchical Silica

Hierarchical silica (HS) was synthesised by following the previously reported method.[25] 2 g of CTAB was dissolved in 280 mL of deionised water in a 500 mL round-bottom flask, followed by the addition of 3.2 mL of aqueous ammonia, 80 mL of diethyl ether, and 40 mL of ethanol, and stirring the mixture for 30 min at room temperature. Subsequently, 10 mL of tetraethyl orthosilicate (TEOS) was added dropwise under continuous stirring, and the reaction was maintained for 4 h at room temperature until a white precipitate formed. The precipitate was collected by centrifugation, washed repeatedly with distilled water and ethanol until the supernatant reached a neutral pH, and then dried at 60 °C for 12 hours. The dried solid was then refluxed in an ethanolic HCl solution (15 mL of 12 N HCl in 120 mL of ethanol) at 70 °C for 24 h to remove the surfactant template. Finally, the material was filtered, washed to neutrality, and dried again at 60 °C for 12 h to obtain hierarchical silica.

2.4. Preparation of Ni/Support

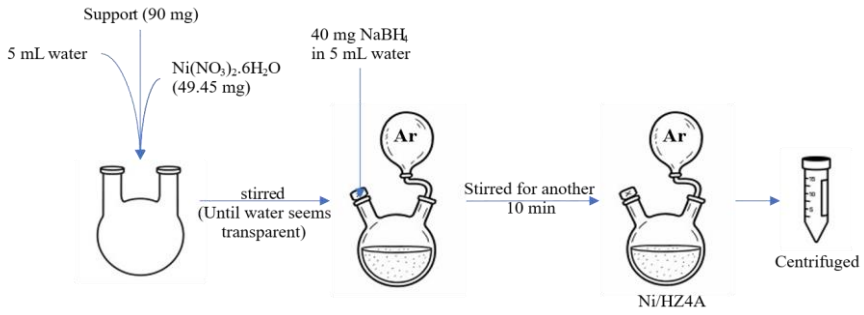


Figure 6. Preparation of the Ni/HZ4A and Ni/HS.

The Ni/Support (10 wt %) catalyst was prepared by wet-impregnation method. 90 mg of Support (HZ4A or HS) was dispersed in 5 mL of distilled water in a 50 mL two-neck round-bottom flask, which was sealed with a stopcock on one neck and an Argon gas balloon on the other. Then, 49.54 mg of $Ni(NO_3)_2 \cdot 6H_2O$ (10 wt % Ni) was added to the suspension, and the mixture was stirred for 12 h and 24 h for HZ4A and HS, respectively. Subsequently, 5 mL of an aqueous $NaBH_4$ solution (40 mg) was added dropwise under an inert atmosphere, followed by stirring for 20 min and sonication for an additional 10 min to ensure complete

reduction. The resulting catalyst was collected by centrifugation, washed three times with water, and stored in a desiccator for further use.

2.5. Lignin Extraction

The extraction of lignin from wheat straw was carried out using the conventional soda pulping process.[6] Before extraction, the wheat straw was thoroughly washed with distilled water to remove adhering dust (water-soluble impurities) and then dried at 60 °C for 24 h. The dried straw was then milled and sieved to obtain a straw Powder. For soda pulping, 10 g of wheat straw was placed in a 250 ml hydrothermal reactor. 80 mL aqueous solution of 5% sodium hydroxide (1:8 mass/liquor) was added. The mixture was heated at 90 °C in a temperature-programmable oven for 3 h. During the cooking process, lignin was solubilised into the black liquor through cleavage of ether linkages and partial depolymerisation of the lignin-carbohydrate complex.

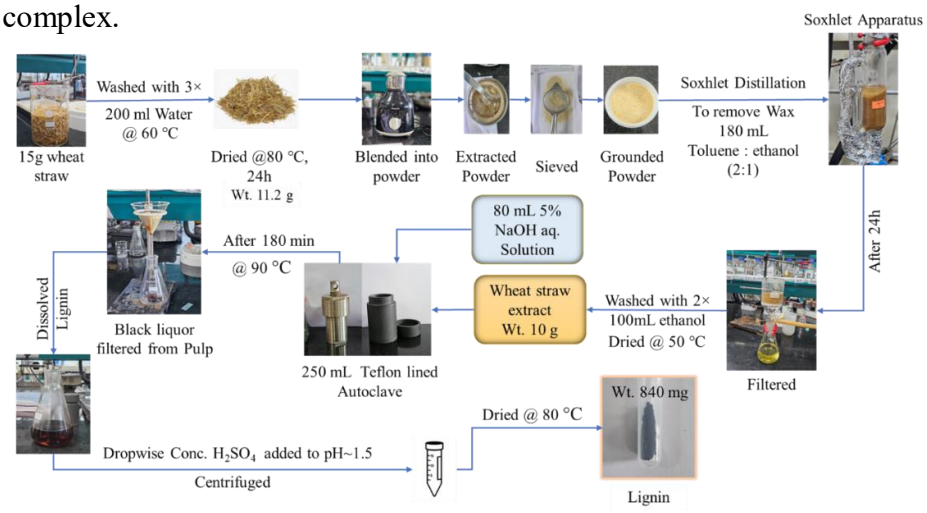
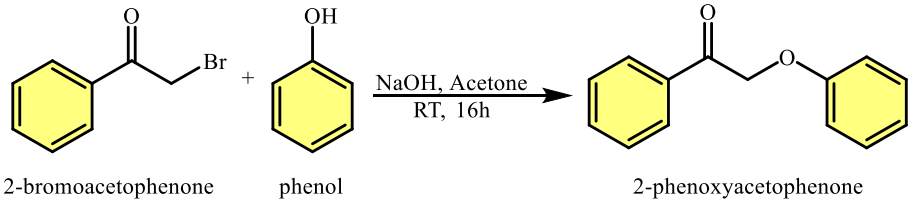


Figure 7 Lignin Extraction by soda pulp method

After the reaction was completed, the slurry was cooled to room temperature and filtered to separate the solid cellulosic residue from the black liquor. The filtrate containing solubilised lignin was adjusted to pH 1.5 using 2M H_2SO_4 under continuous stirring to precipitate lignin. The precipitated lignin was recovered by centrifugation at 7500 rpm for 10 min, washed repeatedly with distilled water until the filtrate reached neutral pH, and subsequently dried overnight at 50 °C under vacuum to obtain purified soda lignin. This yielded 840.3 mg of lignin, equivalent to 8.43% of the oven-dry weight of the wheat straw and around 50% to

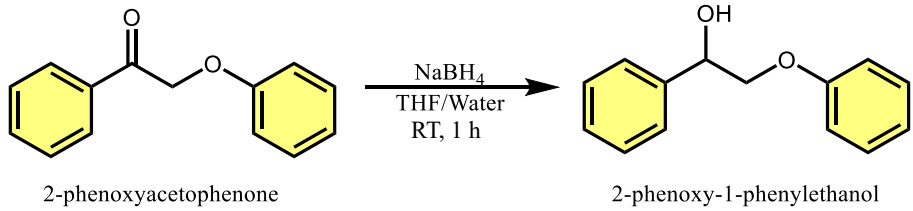
the theoretical yield. The same methods were followed to extract and characterise rice straw lignin. The reaction was repeated on a gram scale to isolate more lignin for further reactions.

2.6. Synthesis of *β*-O-4 model compounds



Scheme 1. Synthesis of *β*-O-4 model compound (Step I)

Under an argon atmosphere, phenol (0.54 g) and K_2CO_3 (0.81 g) were added to acetone (12 mL) and stirred at room temperature for 30 min, followed by the addition of 2-bromoacetophenone (1.09 g). The reaction mixture was stirred at room temperature for 16 h, after which the solids were filtered off, and the filtrate was concentrated under reduced pressure. The residue was dissolved in ethyl acetate (~15 mL), washed with 5% aqueous NaOH (2-3 mL) and water (2-3 mL), dried over anhydrous Na_2SO_4, concentrated, and the product was purified by recrystallization from ethanol.[26]



Scheme 2. Synthesis of *β*-O-4 model compound (Step II)

2-phenoxyacetophenone (100 mg) was dissolved in THF/H_2O (4:1, 5 mL), and $NaBH_4$ (36 mg) was added in one portion, followed by stirring at room temperature for 1 h. The reaction was quenched with saturated NH_4Cl solution (~3 mL), and the mixture was extracted with ethyl acetate (3 × 5 mL). The combined organic layers were washed with brine (10 mL), dried over anhydrous Na_2SO_4, filtered, and the solvent was evaporated to obtain the product.[26]

2.7. Catalytic Reaction

In a typical experiment, 1 mmol of substrate, 40 mg of catalyst, and 5 mL of water were charged into a 10 mL stainless-steel microreactor at room temperature and then sealed. The air inside the reactor was removed by purging with H_2 three times, followed by pressurization to 5 bars. The reaction was carried out at 120 °C for 2 h. After completion, the reactor was cooled to room temperature and carefully depressurized. The reaction mixture was then filtered to separate the catalyst. Product identification was performed using a gas chromatograph equipped with a mass spectrometric detector. Separation was achieved using a capillary column (30 m × 0.25 mm × 0.1 µm film thickness). The oven temperature program commenced at 50 °C (held for 2 min), followed by heating at 8 °C min^{-1} to a final temperature of 290 °C, where it was held for 5 min. The MS ion source was maintained at 230 °C, and data were collected in full-scan mode over a mass range of 40–500 amu.

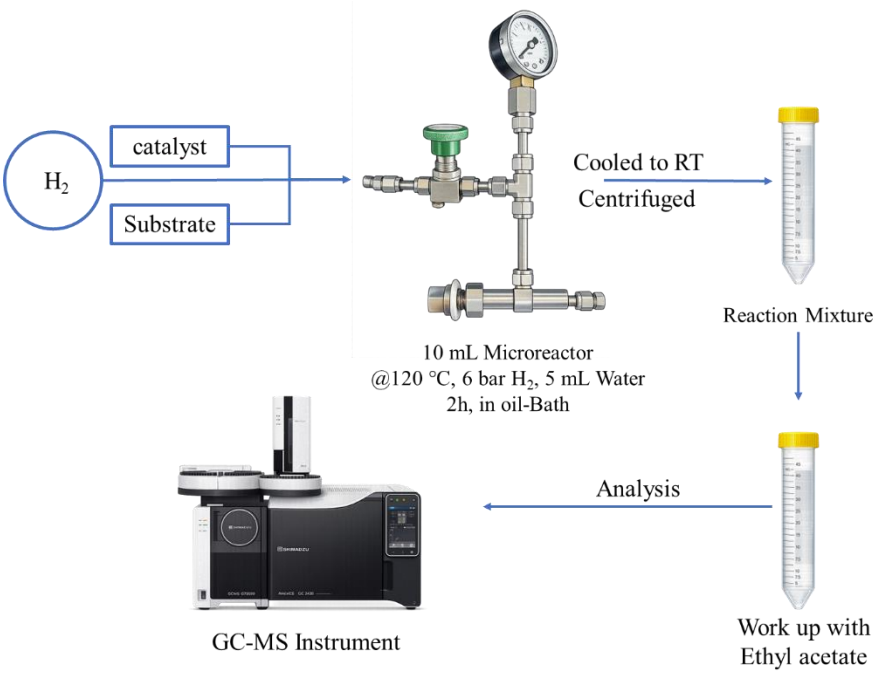


Figure 8. Catalytic reaction procedure

CHAPTER 3

RESULT AND DISCUSSION

3.1. Characterization

The FTIR spectrum of lignin showed a broad O—H stretch at 3427 cm^{-1} and C—H stretching bands at 2936 and 2840 cm^{-1}. A carbonyl peak at 1711 cm^{-1} and aromatic skeletal vibrations at 1600 and 1510 cm^{-1} confirmed the presence of carbonyl groups and an aromatic backbone. Additional features included C—H deformation at 1460 cm^{-1}, guaiacyl C—O stretching at 1265 cm^{-1}, strong Syringyl/guaiacyl C—O bands at 1120–1030 cm^{-1}, and aromatic C—H out-of-plane deformation at 803 cm^{-1}. These signals collectively affirm lignin's complex polyaromatic structure.

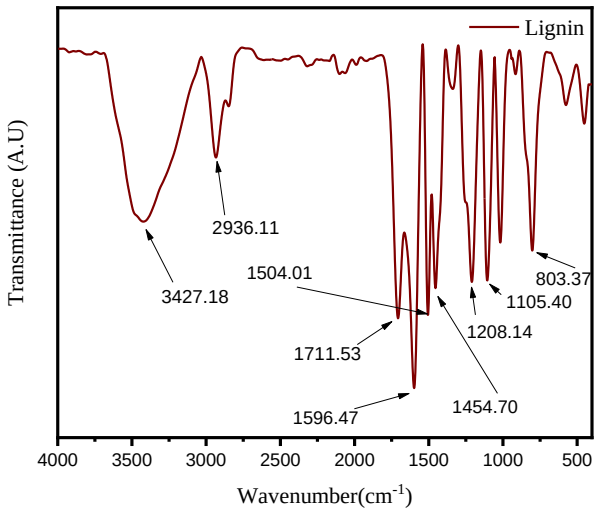


Figure 9. FTIR of Extracted Lignin

FTIR spectrum of HZ4A shows a broad O—H stretching band near 3400 cm^{-1} and an H—O—H bending band at 1630 cm^{-1}, indicating surface hydroxyls and adsorbed water. Strong absorptions at 1050-1130 cm^{-1} correspond to asymmetric Si—O—Si/Si—O—Al stretching, while bands around 790 cm^{-1} and 460 cm^{-1} arise from symmetric Si—O stretching and T—O—T (T: a tetrahedrally coordinated atom, typically Si or Al) bending vibrations, respectively. These features confirm the characteristic aluminosilicate framework of HZ4A (Figure 12a). The same characteristic peaks were observed for Ni/HZ4A, indicating that

the fundamental framework structure of HZ4A remained intact upon metal loading (Figure 12-a,b). Whereas hierarchical silica displays features of a silica framework that in the 1160 cm^{-1} region corresponds to asymmetric Si—O—Si stretching, while the band near 780 cm^{-1} is attributed to symmetric Si—O stretching. A peak around 450 cm^{-1} arises from Si—O—Si bending vibrations (Figure 9-c).

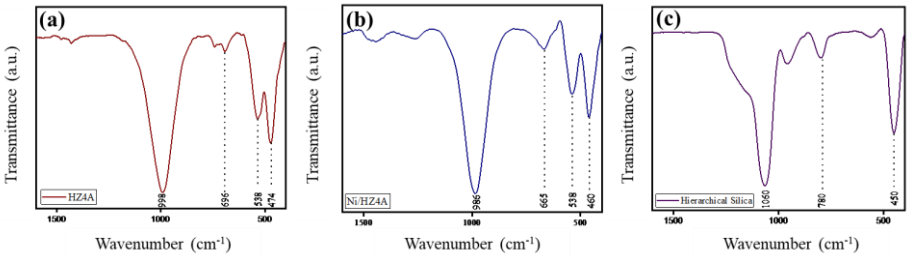


Figure 10. FTIR of (a) HZ4A, (b) Ni/HZ4A, (c) Hierarchical silica,

The P-XRD pattern of HZ4A exhibits several intense reflections, particularly in the 10-30° (2θ) range, confirming its highly ordered crystalline aluminosilicate framework. Beyond 30°, the gradual reduction in peak intensity suggests the presence of a minor amorphous fraction within the material and the data matches with previously reported data.[24,25]

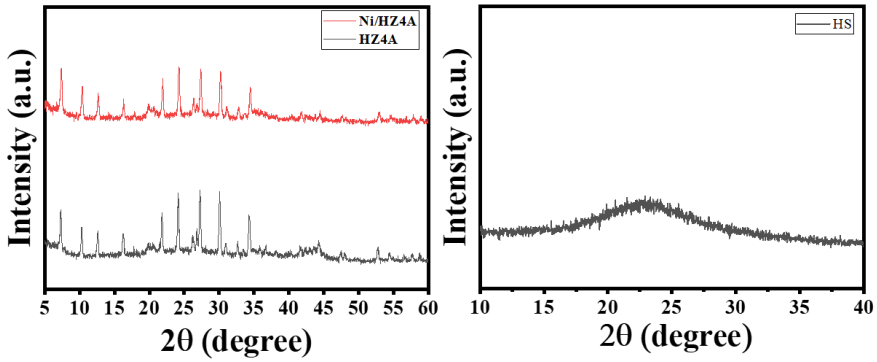
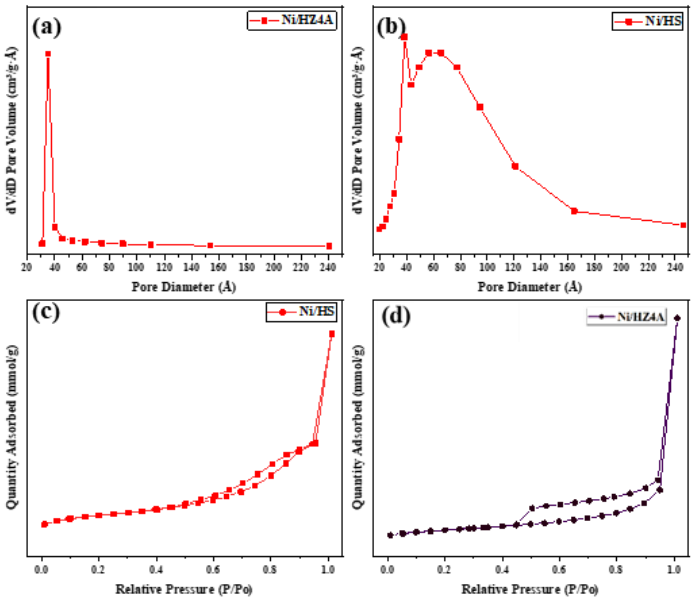


Figure 11. P-XRD of (a) HZ4A, (b) HS



Catalyst	S_{BET} (m^2/g)	V_{total} (cm^3/g)	V_{micro} (cm^3/g)	V_{meso} (cm^3/g)	D(nm)
Ni/HZ4A	83.7311	0.173859	0.001005	0.172854	5.28
Ni/HS	184.4850	0.372138	—	0.372138	7.25

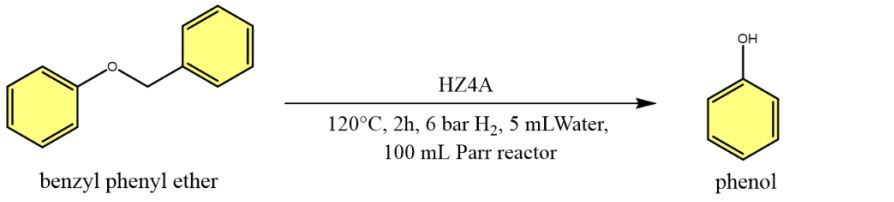
Figure 12. Pore diameter (a-b), and BET data (c-d) of catalysts

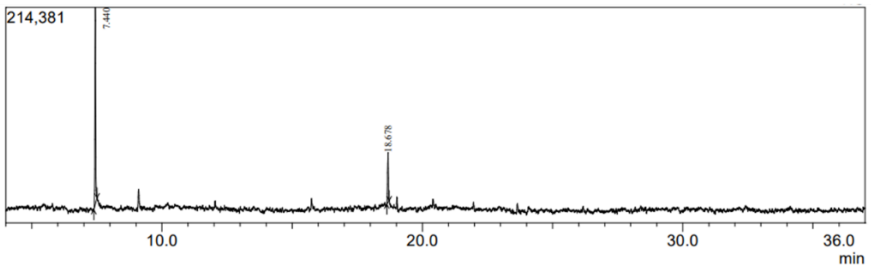
The textural properties of the synthesized catalysts were analysed using N_2 adsorption-desorption measurements based on the BET method. Both Ni/HS and Ni/HZ4A exhibited type IV adsorption-desorption isotherms, confirming the mesoporous nature of the materials. A sharp increase in nitrogen uptake at high relative pressure ($P/P_o > 0.9$) indicated capillary condensation within mesoporous channels. Ni/HS showed a significantly higher BET surface area of 184.49 m^2g^{-1} compared to 83.73 m^2g^{-1} for Ni/HZ4A. The higher surface area of Ni/HS suggests the presence of a greater number of accessible active sites for catalytic reactions. The total pore volume of Ni/HS (0.372 cm^3g^{-1}) was also higher than that of Ni/HZ4A (0.174 cm^3g^{-1}), indicating a more developed porous framework. The average pore diameters of Ni/HS and Ni/HZ4A were found to be 7.25 and 5.28 nm, respectively, confirming the mesoporous structure of both catalysts. Micropore analysis revealed negligible microporous contribution, indicating that mesoporosity predominates in both materials.

3.2. Reaction of Benzyl Phenyl Ether (α-O-4)

3.2.1. With HZ4A under H_2 in a 100 mL High pressure reactor

The conversion of benzyl phenyl ether, α-O-4 model compound over HZ4A at 120 °C under 6 bar H_2 in a 100 mL parr reactor afforded phenol as the dominant product (78.97%), with residual unreacted ether (21.03%).





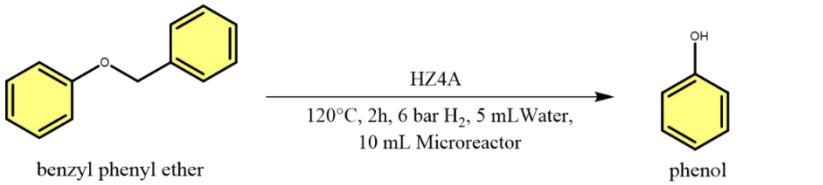
Peak Report TIC

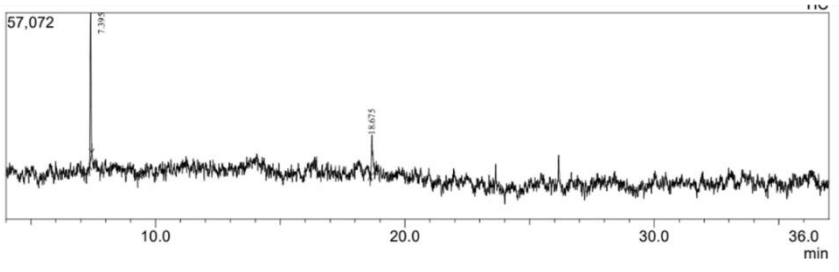
Peak#	R.Time	Area	Area%	Height	Height%	A/H	Name
1	7.440	427231	78.97	195791	79.69	2.18	Phenol
2	18.678	113794	21.03	49901	20.31	2.28	Benzene, (phenoxymethyl)-
		541025	100.00	245692	100.00		

Figure 13. GC-MS data of BPE reaction with HZ4A under H_2 in 100 mL High pressure reactor

3.2.2. With HZ4A under H_2

A comparatively lower phenol yield (65.39%) and a higher fraction of unconverted BPE (34.61%) were observed, when benzyl phenyl ether was reacted with HZ4A in 10 mL microreactor under H_2 atmosphere, indicating incomplete conversion under these conditions.





Peak Report TIC

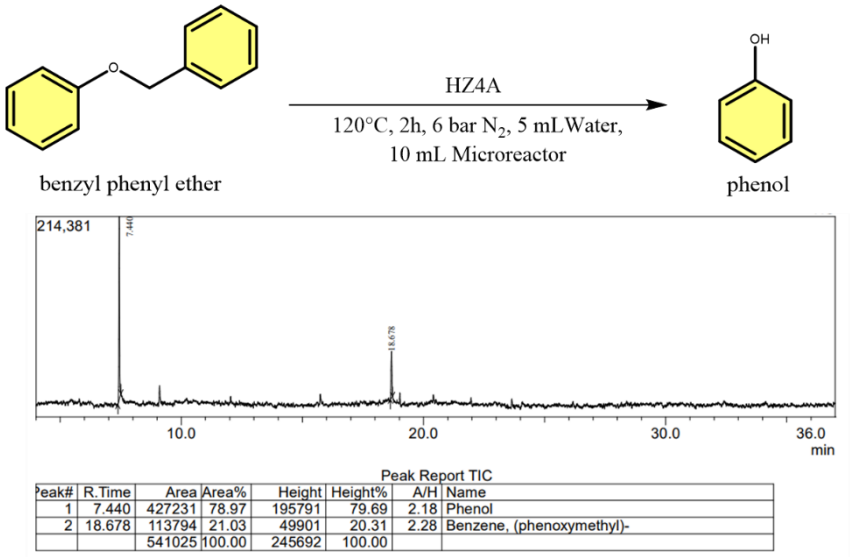
Peak#	R.Time	Area	Area%	Height	Height%	A/H	Name
1	7.395	78489	65.39	40803	78.72	1.92	Phenol
2	18.675	41542	34.61	11032	21.28	3.77	Benzene, (phenoxymethyl)-
		120031	100.00	51835	100.00		

Figure 14. GC-MS data of BPE reaction with HZ4A under H_2

The product distribution remains consistent with acid-driven ether cleavage, though reduced efficiency suggests possible limitations in catalyst accessibility or reaction conditions.

3.2.3. With HZ4A under N_2

Under an inert atmosphere, phenol formation (78.97%) remained comparable to that under hydrogen, showing that without hydrogen ether bond cleavage over HZ4A is possible. This highlights the dominant role of acid catalysis, where C—O bond scission proceeds effectively even in the absence of reductive conditions.



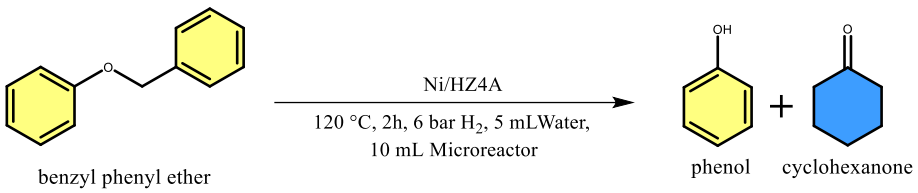
Peak Report TIC

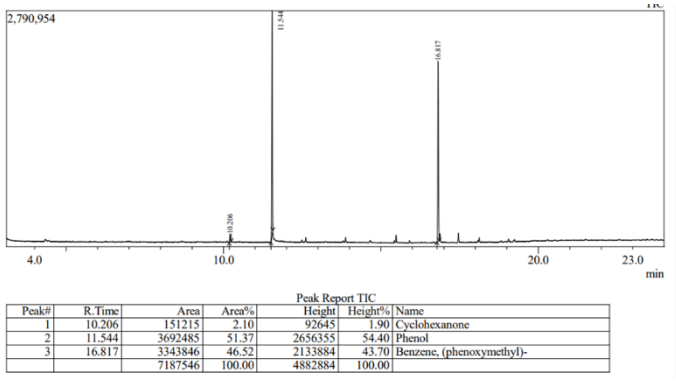
Peak#	R.Time	Area	Area%	Height	Height%	A/H	Name
1	7.440	427231	78.97	195791	79.69	2.18	Phenol
2	18.678	113794	21.03	49901	20.31	2.28	Benzene, (phenoxymethyl)-
		541025	100.00	245692	100.00		

Figure 15. GC-MS data of BPE reaction with HZ4A under N_2

3.2.4. With Ni/HZ4A under H_2

When benzyl phenyl ether (BPE) reacted in presence of bifunctional catalyst system yielded phenol (51.37%), unreacted ether (46.52%), and a minor fraction of cyclohexanone (2.10%). The coexistence of acid and metal sites enables both cleavage and hydrogenation; however, incomplete conversion suggests suboptimal synergy between the components, limiting overall efficiency.





Peak Report TIC

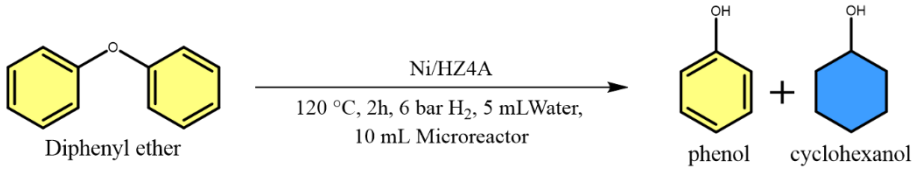
Peak#	R.Time	Area	Area%	Height	Height%	Name
1	10.206	151215	2.10	92645	1.90	Cyclohexanone
2	11.544	3692485	51.37	2656355	54.40	Phenol
3	16.817	3343846	46.52	2133884	43.70	Benzene, (phenoxymethyl)-
		7187546	100.00	4882884	100.00	

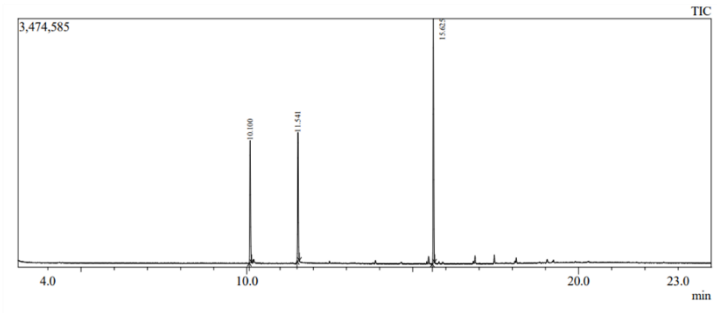
Figure 16. GC-MS data of BPE reaction with Ni/HS under H_2

3.3. Reaction of Diphenyl Ether (4-O-5)

3.3.1. With Ni/HZ4A under H_2

Diphenyl ether conversion resulted in a mixture of phenol (24.42%), cyclohexanone (23.69%), and unreacted diphenyl ether (DPE) (51.88%). The lower conversion compared to BPE reflects the higher stability of the aryl–O–aryl bond. The formation of cyclohexanol confirms the hydrogenation activity of Ni, while partial conversion indicates limited ether bond cleavage efficiency.





Peak Report TIC

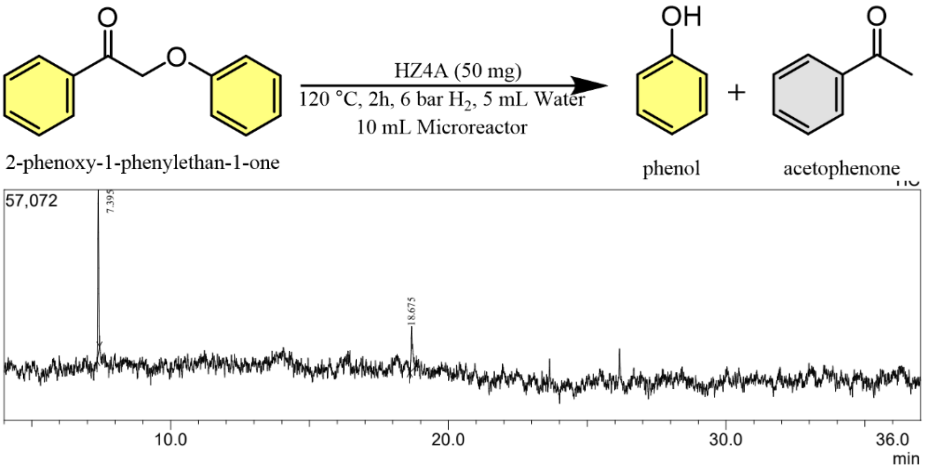
Peak#	R.Time	Area	Area%	Height	Height%	Name
1	10.100	2371504	23.69	1707177	24.68	Cyclohexanol
2	11.541	2444648	24.42	1794275	25.94	Phenol
3	15.625	5193467	51.88	3415705	49.38	Diphenyl ether
		10009619	100.00	6917157	100.00	

Figure 17. GC-MS data of DPE reaction with Ni/HZ4A under H_2

3.4. Reaction of 2-phenoxy-1-phenylethanone (*β*-O-4)

3.4.1. With HZ4A under H_2

The reaction yielded phenol (34.28%) and acetophenone (7.35%), indicating cleavage of the ether linkage accompanied by partial transformation of the carbonyl functionality. The moderate conversion suggests that while HZ4A can promote bond cleavage, the substrate exhibits greater resistance compared to simpler ether models.



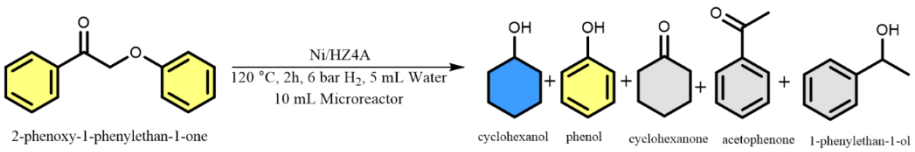
Peak Report TIC

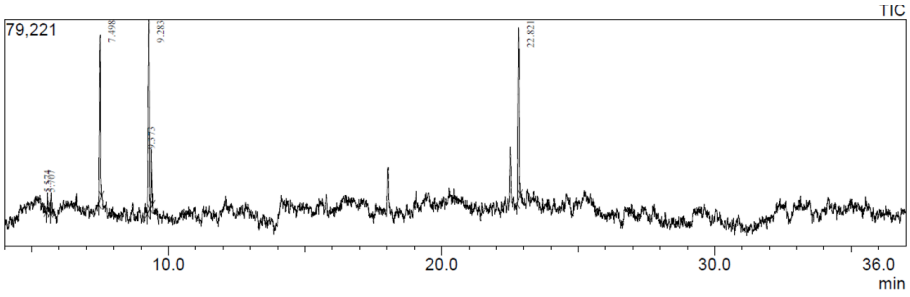
Peak#	R.Time	Area	Area%	Height	Height%	A/H	Name
1	7.395	78489	65.39	40803	78.72	1.92	Phenol
2	18.675	41542	34.61	11032	21.28	3.77	Benzene, (phenoxymethyl)-
		120031	100.00	51835	100.00		

Figure 18. GC-MS data of 2-phenoxy-1-phenylethan-1-one reaction with HZ4A in H_2

3.4.2. With Ni/HZ4A under H_2

Reaction of 2-(2-methoxyphenoxy)-1-phenylethan-1-one with Ni/HZ4A under H2 atomospshere, primarily proceeds via C–O bond cleavage of 2-phenoxy-1-phenylethanone, forming phenol (26.20%) and acetophenone (8.04%). The acetophenone is further hydrogenated to α-methylbenzyl alcohol (33.76%), which constitutes the major product. Minor amounts of cyclohexanol (1.80%) and cyclohexanone (2.13%) suggest limited hydrogenation of the aromatic ring. The presence of a significant fraction of unreacted substrate (28.06%) indicates incomplete conversion under the applied conditions.





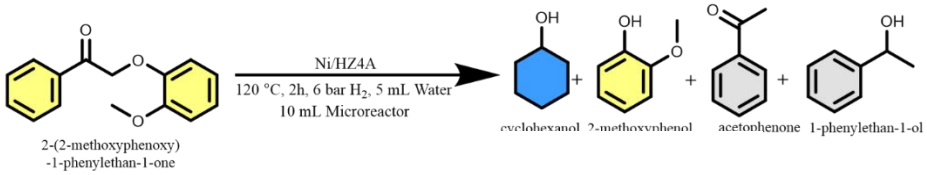
Peak Report TIC

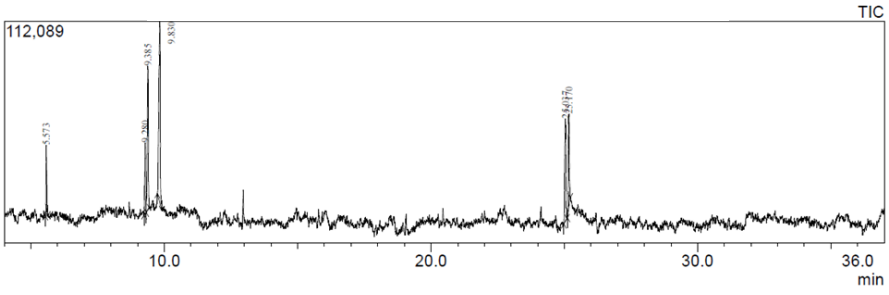
Peak#	R.Time	Area	Area%	Height	Height%	A/H	Name
1	5.574	10189	1.80	6628	3.04	1.54	Cyclohexanol
2	5.707	12073	2.13	7133	3.27	1.69	Cyclohexanone
3	7.498	148404	26.20	57633	26.40	2.57	Phenol
4	9.283	191225	33.76	67003	30.69	2.85	Benzenemethanol, .alpha.-methyl-
5	9.373	45519	8.04	20040	9.18	2.27	Acetophenone
6	22.821	158938	28.06	59855	27.42	2.66	2-Phenoxy-1-phenylethanone
		566348	100.00	218292	100.00		

Figure 19. GC-MS data of 2-phenoxy-1-phenylethan-1-one reaction with Ni/HZ4A in H_2

3.4.3. With Ni/HZ4A in H_2

When 2-phenoxy-1-phenylethan-1-one reacted with Ni/HZ4A in H2, diverse product distribution was observed, including guaiacol (35.16%), acetophenone (22.21%), α-methylbenzyl alcohol (7.63%), cyclohexanol (6.13%), and unreacted substrate (28.87%). The formation of guaiacol confirms selective ether bond cleavage with retention of the methoxy group, while the presence of alcohols and ketones indicates concurrent hydrogenation and carbonyl transformation pathways.





Peak Report TIC

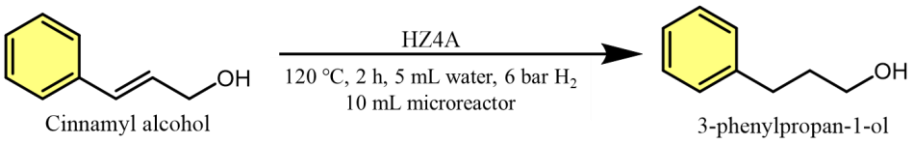
Peak#	R.Time	Area	Area%	Height	Height%	A/H	Name
1	5.573	60857	6.13	35616	10.64	1.71	Cyclohexanol
2	9.280	75789	7.63	35711	10.67	2.12	Benzenemethanol, .alpha.-methyl-
3	9.385	220588	22.21	72726	21.72	3.03	Acetophenone
4	9.830	349194	35.16	91855	27.43	3.80	Phenol, 2-methoxy-
5	25.037	156493	15.76	51934	15.51	3.01	2-Phenoxy-1-phenylethanone
6	25.170	130197	13.11	47000	14.04	2.77	2-Phenoxy-1-phenylethanone
		993118	100.00	334842	100.00		

Figure 20. GC-MS data of 2-(2-methoxyphenoxy)-1-phenylethan-1-one reaction with Ni/HZ4A

3.5. Reaction of monolignol model compounds

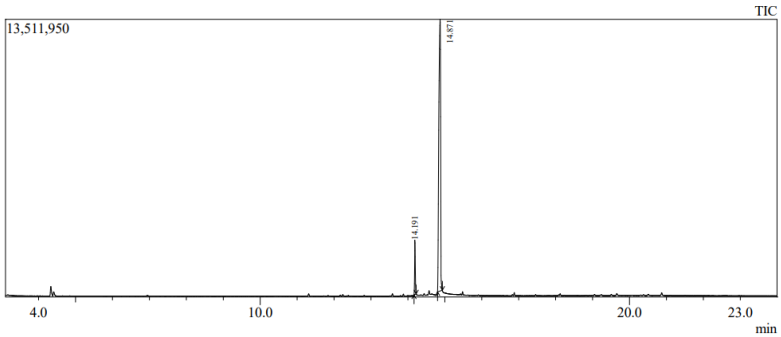
3.5.1. Cinnamyl alcohol with HZ4A under H_2

Reaction of cinnamyl alcohol over the catalyst under H_2 atmosphere showed high selectivity toward cinnamyl alcohol (91.81%), indicating limited conversion of the starting material. A minor product, 3-phenylpropanol (8.19%), was formed via hydrogenation of the C=C bond of cinnamyl alcohol.



Cinnamyl alcohol

3-phenylpropan-1-ol



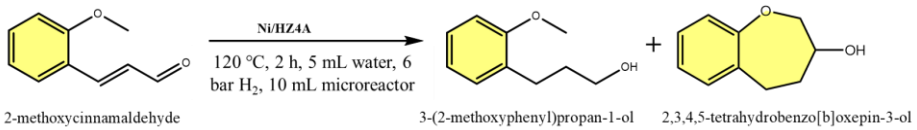
Peak Report TIC

Peak#	R.Time	Area	Area%	Height	Height%	Name
1	14.191	3873320	8.19	2647888	16.69	3-Phenylpropanol
2	14.871	43424493	91.81	13216452	83.31	2-Propen-1-ol, 3-phenyl-
		47297813	100.00	15864340	100.00	

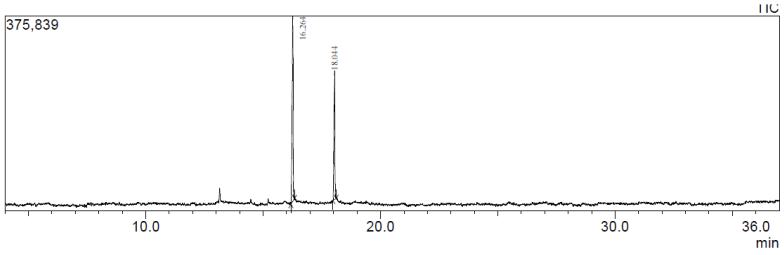
Figure 14 GC-MS data of reaction cinnamyl alcohol with HZ4A

3.5.2. 2-methoxycinnamaldehyde reaction with Ni/HZ4A

Reaction of 2-methoxycinnamaldehyde under H_2 atmosphere predominantly showed selectivity toward 3-(2-methoxyphenyl) propan-1-ol (61.56%), formed via hydrogenation of the C=C bond. A secondary product, 2,3,4,5-tetrahydrobenzo[b]oxepin-3-ol (38.44%), was also observed, indicating partial cyclization during the reaction.



2-methoxycinnamaldehyde 3-(2-methoxyphenyl)propan-1-ol 2,3,4,5-tetrahydrobenzo[b]oxepin-3-ol



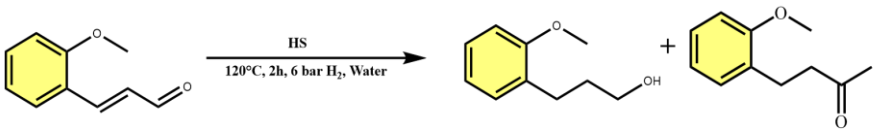
Peak Report TIC

Peak#	R.Time	Area	Area%	Height	Height%	A/H	Name
1	16.264	1091005	61.56	357740	58.98	3.05	Benzenepropanol, 2-methoxy-
2	18.044	681173	38.44	248780	41.02	2.74	1-Benzoxepin-3-ol, 2,3,4,5-tetrahydro-
		1772178	100.00	606520	100.00		

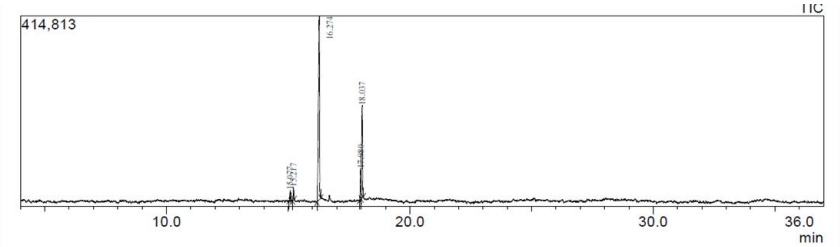
Figure 22. GC-MS data of 2-methoxycinnamaldehyde reaction with Ni/HZ4A

3.5.3. 2-methoxycinnemaldehyde reaction with HS

Reaction of 2-methoxycinnamaldehyde under H_2 atmosphere primarily showed selectivity toward 3-(2-methoxyphenyl) propan-1-ol (23.05%) and 4-(2-methoxyphenyl) butan-2-one (7.69%). Minor products including, indicating partial hydrogenation and rearrangement reactions during the catalytic process.



2-methoxycinnamaldehyde 3-(2-methoxyphenyl)propan-1-ol 4-(2-methoxyphenyl)butan-2-one



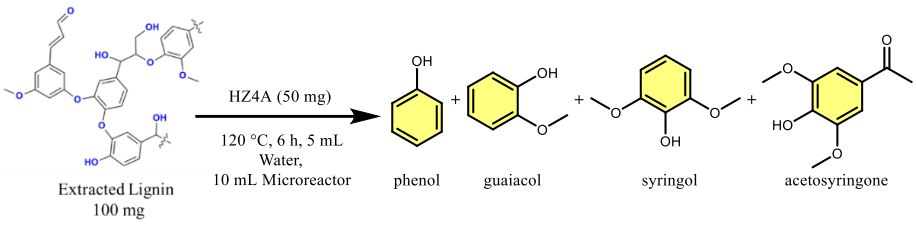
Peak Report TIC

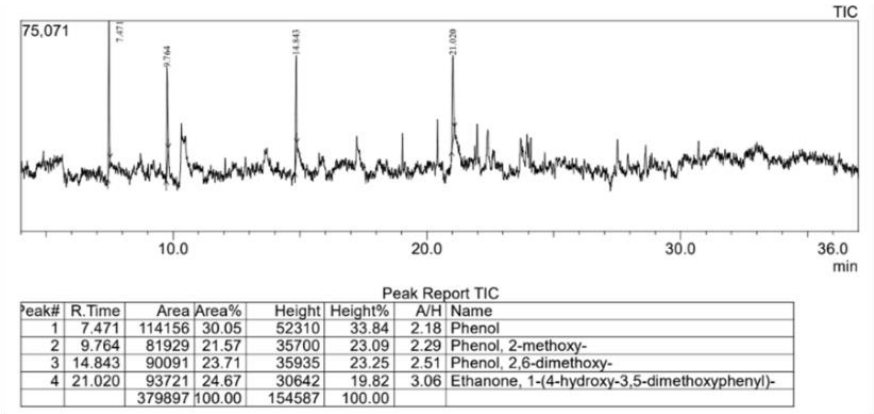
Peak#	R.Time	Area	Area%	Height	Height%	A/H	Name
1	15.077	43667	2.06	23570	3.26	1.85	O-Methoxy-.alpha.-methylbenzyl alcohol
2	15.217	60588	2.86	29021	4.01	2.09	Benzenepropanol, 2-methoxy-
3	16.274	1361272	64.34	400915	55.46	3.40	Benzenepropanol, 2-methoxy-
4	17.980	162711	7.69	67013	9.27	2.43	(Z)-2-Methoxycinnamaldehyde
5	18.037	487608	23.05	202320	27.99	2.41	2-Butanone, 4-(2-methoxyphenyl)-
		2115846	100.00	722839	100.00		

Figure 23. GC-MS data of 2-methoxycinnemaldehyde reaction with HS

3.6. Reaction of Extracted Lignin

3.6.1. With HZ4A under H_2





Peak Report TIC

Peak#	R.Time	Area	Area%	Height	Height%	A/H	Name
1	7.471	114156	30.05	52310	33.84	2.18	Phenol
2	9.764	81929	21.57	35700	23.09	2.29	Phenol, 2-methoxy-
3	14.843	90091	23.71	35935	23.25	2.51	Phenol, 2,6-dimethoxy-
4	21.020	93721	24.67	30642	19.82	3.06	Ethanone, 1-(4-hydroxy-3,5-dimethoxyphenyl)-
		379897	100.00	154587	100.00		

Figure 24. GC-MS data of Lignin with HZ4A catalyst

Depolymerization of lignin yielded a mixture of phenolic monomers, including phenol (30.05%), guaiacol (21.57%), syringol (23.71%), and acetosyringone (24.67%). The broad product distribution reflects cleavage of multiple ether linkages within the lignin matrix, while preservation of methoxy-substituted phenols indicates limited demethoxylation under the applied conditions.

CHAPTER 4

CONCLUSION AND FUTURE SCOPE

In this work, lignin valorisation was explored through the preparation, characterization, and catalytic evaluation of Ni-supported heterogeneous catalysts. Two support systems- HZ4A zeolite and hierarchical silica (HS)- were synthesized and tested on lignin model molecules, including benzyl phenyl ether (α–O–4), diphenyl ether (4-O-5), phenethyl phenyl ether (β–O–4) and monolignols model compounds. The study demonstrates that the catalytic depolymerization of lignin model compounds is strongly dependent on the nature of the catalyst. Acidic catalysts such as HZ4A predominantly facilitate C–O bond cleavage, leading to the selective formation of phenolic products, whereas metal introduce hydrogenation functionality, enabling further transformation of intermediates into alcohols and saturated compounds. The product distributions obtained from GC–MS analysis confirm that both ether bond scission and subsequent hydrogenation reactions govern the overall transformation mechanism. Further this work has strong potential to support the transition toward sustainable fuel technologies and circular bioeconomy systems by converting low-value waste materials into high-value renewable hydrocarbons for future transportation needs, especially in the aviation sector.

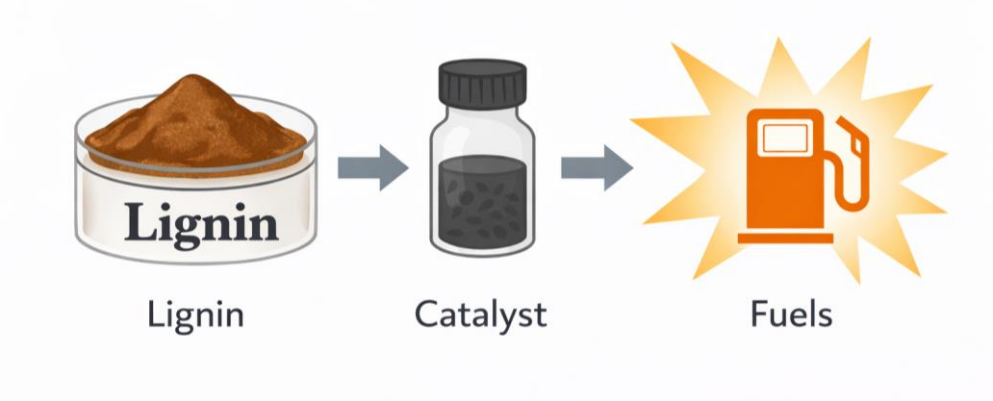


Figure 25. Graphical idea on Lignin to fuel

REFERENCES

1. S. Gundekari, A. Manupathi, S. Chandu, M. Varkolu, P. Kumar, S. K. Karmee, Biomass Convers. Biorefin. **2025**, *15*, 6557-6583.
2. F. Cheng, C. E. Brewer, Renew. Sustain. Energy Rev. **2017**, *72*, 673-722.
3. A. Kamdem Tamo, I. Doench, G. Deffo, S. L. Zambou Jiokeng, G. Doungmo, C. G. Fotsop, R. C. Tonleu Temgoua, A. Montembault, A. Serghei, E. Njanja, I. Kenfack Tonle, A. Osorio-Madrazo, J. Mater. Chem. A **2025**, *13*, 24185-24253.
4. R. S. Abolore, S. Jaiswal, A. K. Jaiswal, Ind. Crops Prod. **2025**, *235*, 121696.
5. X. Lv, C. Zhao, N. Yan, X. Ma, S. Feng, L. Shuai, Bioresour. Technol. **2025**, *419*, 132039.
6. B. Yu, G. Fan, S. Zhao, Y. Lu, Q. He, Q. Cheng, J. Yan, B. Chai, G. Song, Appl. Biol. Chem. **2021**, *64*, 15.
7. V. S. Prabhudesai, L. Gurrala, R. Vinu, Energy Fuels **2022**, *36*, 1155-1188.
8. M. M. Abu-Omar, P. C. Ford, RSC Sustain. **2023**, *1*, 1686-1703.
9. X. Du, S. Wu, P. Li, Bioresources **2023**, *18*, 4231-4261.
10. J. He, L. Lu, C. Zhao, D. Mei, J. A. Lercher, J. Catal. **2014**, *311*, 41-51.
11. H. Konnerth, J. Zhang, M. D., P. M. H. G., Y. Ning, Elsevier **2015**.
12. M. Oregui Bengoechea, A. Hertzberg, N. Miletić, P. L. Arias, T. Barth, J. Anal. Appl. Pyrol. **2015**, *113*, 713-722.
13. Q. Chen, T. Ren, Y. Chai, Y. Guo, I. D. V. Ingram, M. North, H. Xie, Z. Kent Zhao, ChemCatChem **2018**, *10*, 5377-5381.
14. G. Yao, G. Wu, W. Dai, N. Guan, L. Li, Fuel **2015**, *150*, 175-183.
15. S. Li, B. Liu, J. Truong, Z. Luo, P. C. Ford, M. M. Abu-Omar, Green Chem. **2020**, *22*, 7406-7416.
16. A. A. Dwiatmoko, L. Zhou, I. Kim, J. W. Choi, D. J. Suh, J. M. Ha, Catal. Today **2016**, *265*, 192-198.

17. A. Bjelić, M. Grilc, S. Gyergyek, A. Kocjan, D. Makovec, B. Likozar, Catalysts **2018**, *8*, 425.
18. D. P. Phan, E. Y. Lee, Catal. Rev. **2020**, *62*, 607-630.
19. Q. Song, F. Wang, J. Cai, Y. Wang, J. Zhang, W. Yu, J. Xu, Energy Environ. Sci. **2013**, *6*, 994-1007.
20. C. Zhu, J. P. Cao, X. Y. Zhao, T. Xie, J. Ren, X. Y. Wei, J. Energy Inst. **2019**, *92*, 74-81.
21. B. Biswas, M. Sakhakarmy, T. Rahman, H. Jahromi, S. Adhikari, B. B. Krishna, T. Bhaskar, J. Baltrusaitis, M. Eisa, S. M. T. Kouzehkanan, T. S. Oh, Bioresour. Technol. **2024**, *398*, 130517.
22. C. Zhu, J. P. Cao, X. Y. Zhao, T. Xie, J. Ren, X. Y. Wei, J. Energy Inst. **2019**, *92*, 74-81.
23. F. Lin, Y. Ma, Y. Sun, X. Men, Y. Zhu, T. Gao, K. Zhao, Appl. Catal. A Gen. **2020**, *598*, 117552.
24. D. Panda, E. A. Kumar, S. K. Singh, J. CO2 Util. **2020**, *40*, 101223.
25. V. Kulkarni, J. Parthiban, S. K. Singh, Microporous Mesoporous Mater. **2024**, *368*, 112998.
26. J. M. Nichols, L. M. Bishop, R. G. Bergman, J. A. Ellman, J. Am. Chem. Soc. **2010**, *132*, 12554-12555.